DOI: 10.1002/chem.200700069

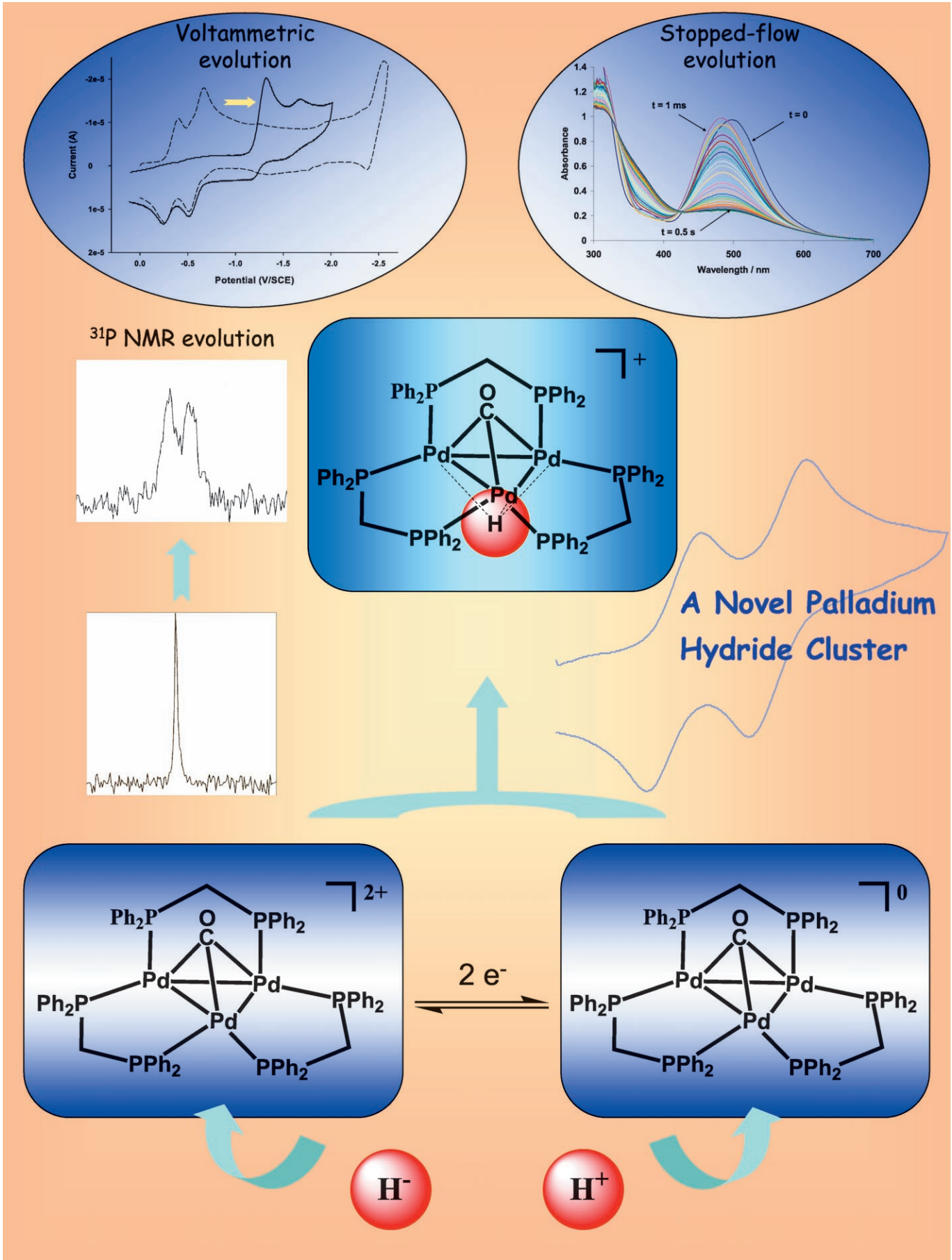

Generation, Characterization, and Electrochemical Behavior of the Palladium–Hydride Cluster $[Pd_3(dppm)_3(\mu_3\text{-}CO)(\mu_3\text{-}H)]^+$ (dppm = Bis(diphenylphosphinomethane)

Cyril Cugnet,[a] Dominique Lucas,*[a] Edmond Collange,[a] Bernard Hanquet,[a] Alain Vallat,[a] Yves Mugnier,[a] Armand Soldera,[b] and Pierre D. Harvey*[b]

Abstract: Addition of formate on the dicationic cluster $[Pd_3(dppm)_3(\mu_3\text{-}CO)]^{2+}$ (dppm = bis(diphenylphosphinomethane) affords quantitatively the hydride cluster $[Pd_3(dppm)_3(\mu_3\text{-}CO)(\mu_3\text{-}H)]^+$. This new palladium–hydride cluster has been characterised by ^1H NMR, ^{31}P NMR and UV/Vis spectroscopy and MALDI-TOF mass spectrometry. The unambiguous identification of the capping hydride was made from ^2H NMR spectroscopy by using DCO_2^- as starting material. The mechanism of the hydride complex formation was investigated by UV/Vis stopped-flow methods. The kinetic data are consistent with a two-step process involving: 1) host–guest interactions between HCO_2^- and $[Pd_3(dppm)_3(\mu_3\text{-}CO)]^{2+}$ and 2) a reductive elimination of CO_2. Two alternatives routes to the hydride complex were also examined : 1) hydride transfer from $NaBH_4$ to $[Pd_3(dppm)_3(\mu_3\text{-}CO)]^{2+}$ and 2) electrochemical reduction of $[Pd_3(dppm)_3(\mu_3\text{-}CO)]^{2+}$ to $[Pd_3(dppm)_3(\mu_3\text{-}CO)]^0$ followed by an addition of one equivalent of H^+. Based on cyclic voltammetry, evidence for a dual mechanism (ECE and EEC; E = electrochemical (one-electron transfer), C = chemical (hydride dissociation)) for the two-electron reduction of $[Pd_3(dppm)_3(\mu_3\text{-}CO)(\mu_3\text{-}H)]^+$ to $[Pd_3(dppm)_3(\mu_3\text{-}CO)]^0$ is provided, corroborated by digital simulation of the experimental results. Geometry optimisations of the $[Pd_3(H_2PCH_2PH_2)_3(\mu_3\text{-}CO)(\mu_3\text{-}H)]^n$ model clusters were performed by using DFT at the B3LYP level. Upon one-electron reductions, the Pd–Pd distance increases from a formal single bond ($n=+1$), to partially bonding ($n=0$), to weak metal–metal interactions ($n=-1$), while the Pd–H bond length remains relatively the same.

Keywords: cluster compounds · electrochemistry · hydrides · kinetics · palladium

Introduction

The Pd–H species are fascinating materials whether they are in the solid state or as organometallics in solution. Numerous solid-state properties such as superconductivity,[1] heterogeneous catalysis[2,3] or electrode materials as films[4] or bulk,[5–7] structures[8] and hydrogen mobility[9,10] have thoroughly been investigated. Pd–H organometallics are suspected to be key intermediates in many homogeneous catalytic processes.[11–17] In fact, recent direct evidence for their existence in solution for these catalytic processes were provided.[18,19] Often, the link between solid-state materials and soluble organometallics passes through the investigation of cluster species as models. Unfortunately, low-valent polynuclear complexes of Pd–H are relatively unstable and therefore rare.[20] The few examples include several dinuclear species so far.[20] However, their importance have attracted some attention on a quantum theoretical point of view in an attempt to shine light on what may happen at the surface or in the bulk during heterogeneous catalytic processes.[21] The first confidently characterised Pd–H clusters were only recently reported,[22,23] and since their characterisation as the tetranuclear clusters $[Pd_4(dppm)_4(\mu\text{-}H)_x]^{x+}$ (**A**: $x=1$; **B**: $x=2$), their properties were also investigated in

[a] C. Cugnet, Dr. D. Lucas, Dr. E. Collange, Dr. B. Hanquet, Dr. A. Vallat, Prof. Y. Mugnier
Institut de Chimie Moléculaire de l'Université de Bourgogne (ICMUB)
UMR CNRS 5260, Faculté des Sciences Mirande
Université de Bourgogne, 9 avenue Alain Savary
21000 Dijon (France)
Fax: (+33) 380-396-065
E-mail: Dominique.Lucas@u-bourgogne.fr

[b] Prof. A. Soldera, Prof. P. D. Harvey
Département de Chimie, Université de Sherbrooke
Sherbrooke, Québec, J1K 2R1 (Canada)
Fax: (+1) 819-821-8017
E-mail: pierre.harvey@USherbrooke.ca

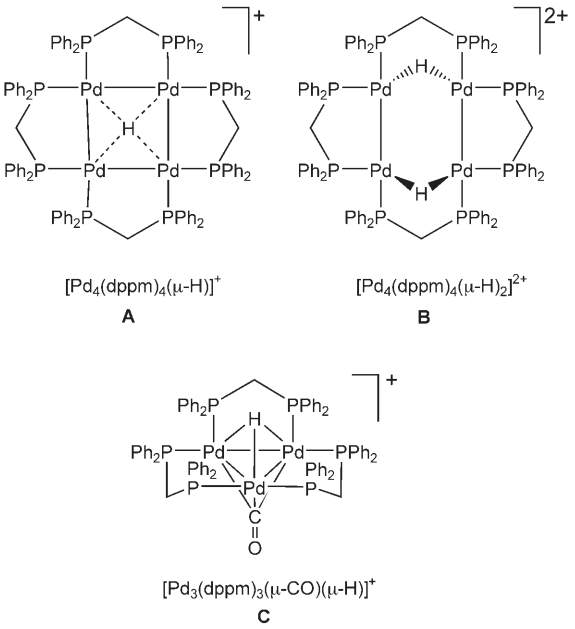

detail and reviewed.[23–27] Belonging to this family, the 44-electron $[Pd_3(dppm)_3(\mu\text{-}CO)(\mu\text{-}H)]^+$ cluster (**C**, $[Pd_3(H)]^+$) was unknown until now, despite the fact past attempts were made to prepare it and that the Pt analogue was well characterised.[28]

We now wish to report the thermal and electrochemical generation of the title clusters along with their characterisation and reactivity. These species represent unique models for the absorption of hydrogen onto the Pd(111) surface. During the course of this study the optimised geometries for $[Pd_3(H)]^n$ ($n=+1$, 0, -1) as well as their qualitative MO analyses are presented.

Results and Discussion

Synthesis and characterisation: Reaction of the dicationic cluster $[Pd_3(dppm)_3(\mu\text{-}CO)]^{2+}$ (dppm = bis(diphenylphosphinomethane, noted $[Pd_3]^{2+}$; PF_6^- as counterion) with tributylammonium formate affords the hydride adduct $[Pd_3(H)]^+$ [Eq. (1)]

$$[Pd_3]^{2+} + HCO_2^- \rightarrow [Pd_3(H)]^+ + CO_2 \quad (1)$$

The formate is a soft hydride donor, which was previously used with success for the synthesis of the tetranuclear $[Pd_4(dppm)_4H_2]^{2+}$.[25] The formate reagent is conveniently prepared by mixing stoichiometric amounts of formic acid and tributylamine [Eq. (2)].

$$Bu_3N + HCO_2H \rightarrow Bu_3NH^+, HCO_2^- \quad (2)$$

The reaction proceeds readily and cleanly. However, $[Pd_3(H)]^+$ is unstable and extensive decomposition occurs when left standing in solution for a period of time exceeding several hours. So its isolation in a pure state is illusive. Therefore, all characterisations were performed on freshly prepared solutions of $[Pd_3(H)]^+$.

The $^{31}P\{^1H\}$ spectrum of $[Pd_3(H)]^+$ displays a single resonance, which is consistent with a C_3-symmetry structure. The chemical shift is located at -12.7 ppm in the range expected for an anion adduct of $[Pd_3]^{2+}$. Further evidence of the hydride was provided by disabling the device for the decoupling of ^1H nucleus (see Figure 1), which results in the splitting of the singlet at -12.7 ppm in two sets of signals with a separation of 19–20 Hz. This value is too high to arise from $^2J(P,H)$ or $^3J(P,H)$ couplings through one or two carbon linkers of the dppm ligand. Instead, a $^2J(P,H)$ coupling between the six equivalent phosphorus nuclei and the hydride through the palladium atoms is a better explanation. For comparison in the Pt series, the hydride in $[Pt_3(dppm)_3(\mu_3\text{-}H)]^+$ gives rise to $^2J(P,H) = 23$ Hz.[28]

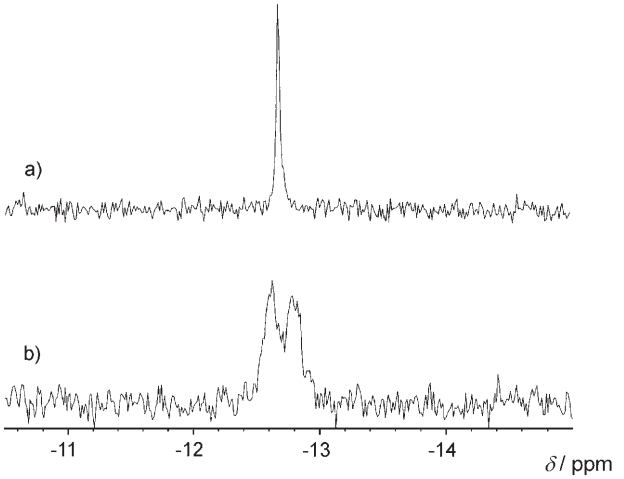

Figure 1. ^{31}P NMR spectrum of $[Pd_3(H)]^+$ in THF/C_6D_6 (50/50): a) ^1H decoupled, b) no decoupling.

The ^1H NMR spectrum exhibits resonances due to the phenyl protons in the range 7.3–8 ppm. The set of two signals at 4.8 and 4.9 ppm is the characteristic pattern observed for the CH_2P_2 protons when both sides of the Pd_3 plane are inequivalent.[29] However, the septet expected for the hydride (coupling with six equivalent ^{31}P nuclei) is yet to be found. It is anticipated that this weak signal (intensity of one H distributed between the seven peaks) is hidden under the stronger resonances of the Bu_3NH^+ co-product, which virtually screens the spectral window between 1 and 4 ppm.

In order to avoid this interference, the reaction [Eq. (3)] was monitored by ^2H NMR spectroscopy.

$$[Pd_3]^{2+} + DCO_2^- \rightarrow [Pd_3(D)]^+ + CO_2 \quad (3)$$

The formate solution was analysed before and after addition of an equimolar amount of the cluster. The initial narrow singlet due to formate DCO_2^- ($\delta = 8.5$ ppm) was replaced by a broad signal at higher field ($\delta = 3.1$ ppm; half-

width = 19 Hz), which was identified as the deuteride. As expected, this chemical shift falls into the Bu_3NH^+ window and explains why the hydride signal is unobserved in the ^1H NMR spectrum. This resonance is placed at unusually high field due the presence of deshielding regions of the Ph groups pointing inward the cavity in which the hydride is located. Pudephatt and collaborators found this signal at −1.04 ppm for the Pt analogue.[28] It is not surprising that the P–D coupling is unresolved, since, relative to P–H, it is reduced by a factor equal to the ratio of the magnetogyric ratios : 6.5144 ($\frac{^2J(P,D)}{^2J(P,H)}=\frac{\gamma_D}{\gamma_H}=\frac{4.1066}{26.7522}$).

In the MALDI-TOF mass spectrum, the highest peak at *m/z* 1472 corresponds to the $Pd_3(dppm)_3$ fragment, confirming that the trinuclear structure is unaffected by the reaction. No fragment was observed that contained the axial ligand CO or H^-, as is usual with this sort of compound.

Mechanistic investigation: The mechanism depicted in Scheme 1 was postulated.

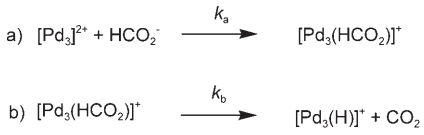

Scheme 1.

It consists of two elementary steps: 1) the binding of formate to the Pd_3 moiety, owing to the strong affinity of the dicationic cluster towards anionic species, particularly carboxylates[30] and 2) from this intermediate, extrusion of CO_2 to afford the hydride complex, a reaction that has many precedents in the literature.[31]

Stopped-flow experiments were carried out to get evidence on this mechanism. This technique allowed the monitoring of the visible spectrum of the reacting mixture over short time periods. The use of different amounts of excess HCO_2^- was tested ($R_0=\frac{[HCO_2^-]t=0}{[Pd_3^{2+}]t=0}$ varying from 10 to 50).

Figure 2 is representative of the evolution of the visible spectrum. Two stages are clearly distinguished: in the first most rapid one, the absorption band of the initial cluster is slightly shifted to the left, which is a typical feature observed when an anionic guest enters into the cavity of the cluster. In the second slower process, this new band decreases and stabilises at nearly one fifth of its initial intensity.

The overall spectrum evolution, analysed by Specfit,[32] matches well the two consecutive step mechanism. Whatever is the excess of formate, all experiments led to nearly the same value of k_b ($10.4\pm0.1\ s^{-1}$). On the contrary, a large discrepancy was obtained between the different experiments for the apparent rate constant k_{obsa}. Indeed, Figure 3 shows the linear dependence of k_{obsa} on $[HCO_2^-]$, in accordance with the first order in formate of step a. This plot allows us to extract the intrinsic rate constant k_a ($4.3\pm0.8\times10^5\ mol^{-1}\,L\,s^{-1}$).

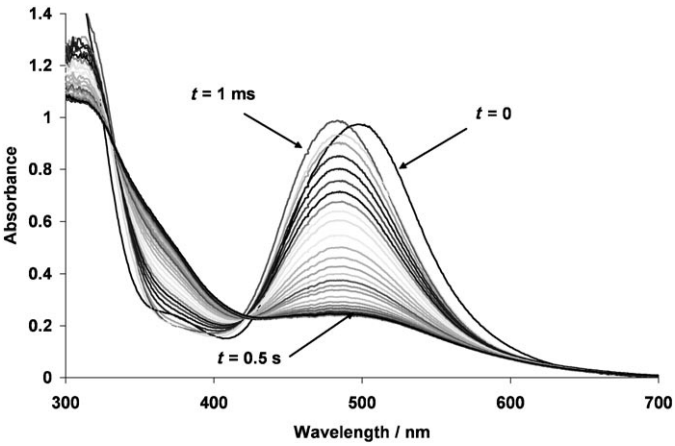

Figure 2. Time evolution of the visible spectrum of the mixture of $[Pd_3]^{2+}$ and HCO_2^- in THF. $[Pd_3^{2+}]_0=2.5\times10^{-4}\ mol\,L^{-1}$ and $R_0=20$.

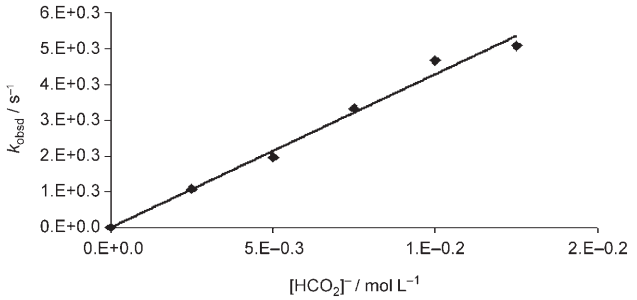

Figure 3. Plot of k_{obsd} as a function of $[HCO_2^-]$.

The spectra of both the intermediate formate and final hydride adducts were recalculated with Specfit (Figure 4). For the former, the absorption maximum is found at 484 nm. For comparison purpose, this maximum is also found at 484 nm for the stable acetate adduct $[Pd_3(CH_3CO_2)]^+$. This argues favourably for the identity of the putative formate intermediate.

Electrochemistry of $[Pd_3(H)]^+$: The reaction was also monitored by rotating disk electrode (RDE) voltammetry analy-

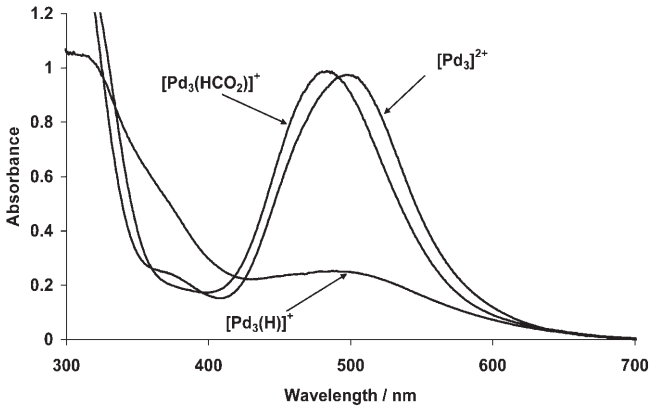

Figure 4. Recalculated spectra of the different participants in Scheme 1.

sis as shown in Figures 5 and 6a. In Figure 5 curve a corresponds to $[Pd_3]^{2+}$ with its two characteristic one-electron reduction waves A_1 and A_2 located at -0.29 and -0.55 V

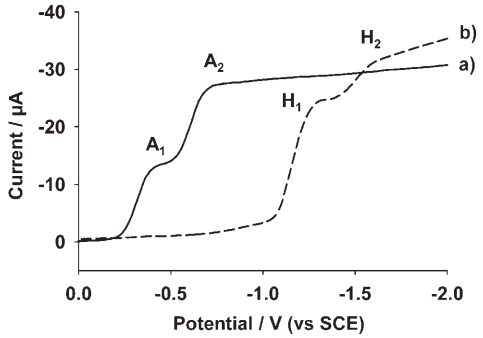

Figure 5. RDE voltammogram of $[Pd_3]^{2+}$ in THF: a) alone; b) after addition of one molar equivalent of NBu_3 and HCO_2H.

(half-wave potentials).[33] Addition of one equivalent of HCO_2^- and subsequent formation of $[Pd_3(H)]^+$ results in complete disappearance of A_1 et A_2 (curve b) that are replaced by two new reduction waves H_1 and H_2 ($E_{1/2} = -1.15$ and -1.5 V). The negative shift in reduction potential is consistent with an increase in electron density at the Pd_3 center due to hydride coordination as observed in the halide adducts.[30]

The CV of $[Pd_3(H)]^+$ is depicted in Figure 6b–d at various scan rates. Peaks H_1 and H_2 appear in the forward scan, with a current ratio in the same range as in RDE voltammetry. In the backward scan, at low scan rates (Figure 6c and d), the corresponding oxidation peaks H'_1 and H'_2 are not observed: the two reduction processes are not reversible, which means that in each case a chemical reaction is coupled to the electron-transfer step. At higher scan rate (Figure 6b), a slight peak H'_1 is observed: evidently, the chemical reaction is no longer totally effective, because of its limited kinetics. Peaks A'_1 and A'_2, assigned to the oxidation of $[Pd_3]^0$ appear also in the reverse scan, demonstrating that the neutral species is the sole product in the reduction process. Electrolyses were performed at either the potential of waves H_1 or H_2. In each case, the reduction operates with a transfer of two Faradays per mol of $[Pd_3(H)]^+$. The resulting RDE voltammogramm displays only the A'_1 and A'_2 waves, showing that $[Pd_3]^0$ is the sole species in solution. This product, related to a two-electron transfer, is consistent with the release of a hydride ion H^-.

Hence, the electrochemical behaviour of $[Pd_3(H)]^+$ is highly reminiscent of that of $[Pd_3(I)]^+$[34] and can be described as a six-member, fence-like square scheme, in which the electron-transfer steps are written horizontally and the H^- exchange equilibrium vertically (Scheme 2).

From this scheme, there are two possible pathways for the reduction of $[Pd_3(H)]^+$ to $[Pd_3]^0$, either EEC (a→b→c→f) or ECE (a→b→e→f). It is worth noting that steps a→b and e→f occur at the potential of H_1 and b→c at the potential of H_2 ($E^o_{e/f} > E^o_{a/b} > E^o_{b/c}$). Hence, a pure EEC mechanism

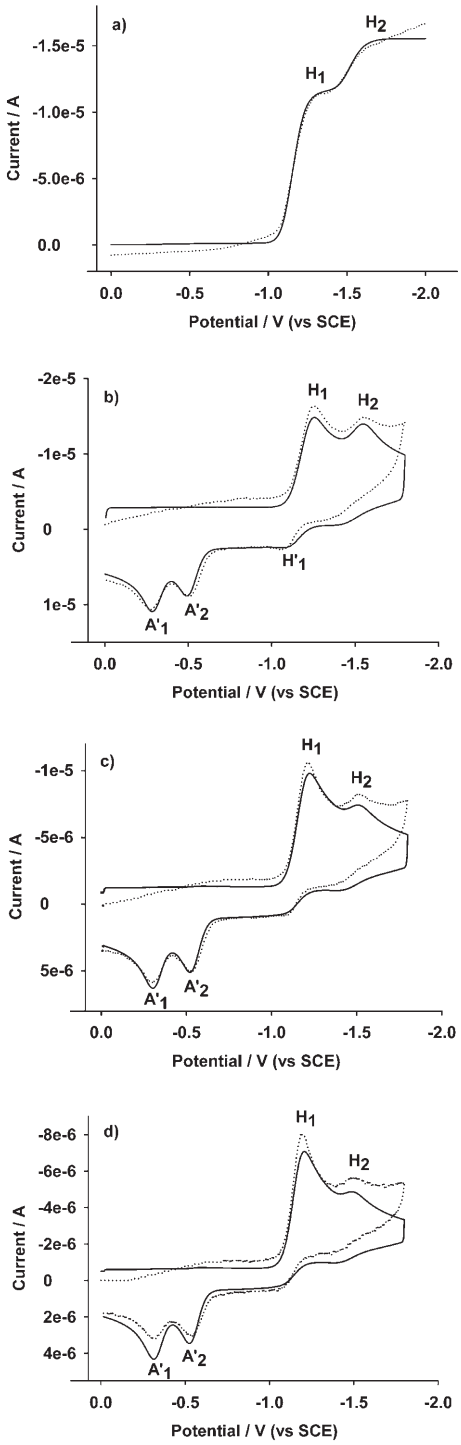

Figure 6. Digital simulations (solid lines) compared to experimental (dotted) RDE and CV scans of $[Pd_3(H)]^+$ in THF. Concentration of $[Pd_3(H)]^+$: a) 6.8 mM; b)–d) 6.3 mM. Scan rates: a) 20 mV s^{-1}; b) 300 mV s^{-1}; c) 100 mV s^{-1}; d) 50 mV s^{-1}. Electrode: material = vitreous carbon; diameter = 3 mm; a) angular velocity = 26.5 rad s^{-1}.

would lead to reduction peaks (or waves) H_1 and H_2, of similar current magnitude, each corresponding to a one-electron transfer. Conversely, the sole ECE pathway would give the single two-electron peak (or wave) H_1. In fact, both peaks

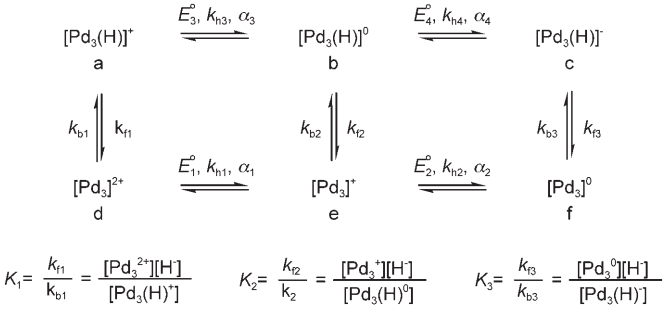

$$K_1 = \frac{k_{f1}}{k_{b1}} = \frac{[Pd_3^{2+}][H^-]}{[Pd_3(H)^+]} \qquad K_2 = \frac{k_{f2}}{k_2} = \frac{[Pd_3^{+}][H^-]}{[Pd_3(H)^0]} \qquad K_3 = \frac{k_{f3}}{k_{b3}} = \frac{[Pd_3^{0}][H^-]}{[Pd_3(H)^-]}$$

Scheme 2.

H_1 and H_2 are observed, but H_2 is of lower current intensity than H_1, which strongly suggests that both mechanisms operate simultaneously. For the reverse oxidation of $[Pd_3]^0$ to $[Pd_3(H)]^+$, the EEC pathway (f→e→d→a), occurring through peaks A'_2 and A'_1, is nearly exclusive. At high sweep rates, the peak H'_1 provides evidence for the presence of $[Pd_3(H)]^0$, from which the loss of H^- is incomplete, near the electrode.

The CV and RDE voltammograms of $[Pd_3(H)]^+$ were simulated with DIGISIM assuming the six-species square scheme shown in Scheme 2. With the parameters listed in Table 1, a satisfying agreement between theoretical and experimental curves is obtained, so corroborating the proposed mechanism. As outlined above, the equilibrium constant K_2 (b⇄e) and the rate constant k_{f2} (b→e) are determining factors in the partition between the two reduction mechanisms EEC and ECE. Notably, a half life time of 0.3 s for $[Pd_3(H)]^0$ is calculated from k_{f2}: in fact, this value is significantly high and explains why the loss of H^- from this species is only partially effective on the voltammetric timescale. The low values of K_1 and k_{f1} confirm that $[Pd_3(H)]^+$ is essentially undissociated in THF. The high values found for K_3 and k_{f3} are consistent with the transient state of $[Pd_3(H)]^-$.

Table 1. Best fit parameters for the digital simulations of the electrochemical experiments on $[Pd_3(H)]^+$.

i[a]	E_i^o [V]	k_{hi} [cm s^{-1}][b]	α_i[c]	K_i [mol L^{-1}][d]	k_{fi} [s^{-1}][e]
1	−0.295	0.2	0.5	1.6×10^{-8}	0.01
2	−0.54	0.2	0.5	4.5×10^{6}	2
3	−1.15	0.005	0.5	7.5×10^{22}	100
4	−1.5	0.005	0.5		

[a] i = integer value used to identify the individual best fit parameters. [b] k_{hi} = heterogeneous charge-transfer rate constants. [c] α_i = charge-transfer coefficients. [d] K_i = equilibrium constants. [e] k_{fi} = chemical reaction constants.

Other routes to the hydride complex: Other reactants were examined as hydride donors. $NaBH_4$, which was successfully used by Puddephatt and collaborators to prepare the Pt analogue,[28] was first attempted. The reaction performed in THF led to $[Pd_3H]^+$ (detected by ^{31}P NMR spectroscopy), but in lower yield (≈85%) than by the formate method.

An alternative route to form the M–H bond is the oxidative addition of H^+ on low-valent metal complexes. In the Pt series, access to $[Pt_3(\mu_3\text{-}H)]^+$ was also provided by reduction of $[Pt_3]^{2+}$ followed by protonation with NH_4PF_6.[28]

The neutral $[Pd_3]^0$ was generated by reductive electrolysis of $[Pd_3]^{2+}$ at the controlled potential of −1 V. Its RDE voltammogramm (Figure 7b) shows the two-oxidation waves

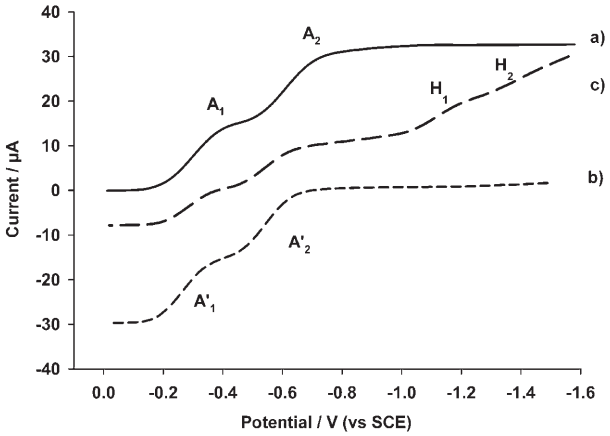

Figure 7. RDE voltammogram of $[Pd_3]^{2+}$ in THF: a) alone; b) after bielectronic reduction by electrolysis at −1 V; c) after addition of two molar equivalents of HPF_6.

A'_1 and A'_2. Addition of excess HPF_6 (two equivalents) provides an RDE voltammogramm (Figure 7c) which shows that two products are now present in solution: $[Pd_3]^+$ is evidenced by waves A'_1 and A_2 and waves H_1 and H_2 can be assigned to $[Pd_3(H)]^+$. The simultaneous formation of these two products occurs through two competitive reactions: 1) protonation of $[Pd_3]^0$ to form the hydride complex [Eq. (4)] and 2) oxidation of $[Pd_3]^0$ by H^+ [Eq. (5)].

$$[Pd_3]^0 + H^+ \rightarrow [Pd_3(H)]^+ \quad (4)$$

$$2[Pd_3]^0 + 2H^+ \rightarrow 2[Pd_3]^+ + H_2 \quad (5)$$

Two convergent mechanisms may account for the reaction given in Equation (5): 1) A direct outer-sphere process, thermodynamically favoured on the basis of the oxidation and reduction potentials of respectively $[Pd_3]^0$ and H^+ ($E^o_{H^+/H_2}$ = 0 V vs. NHE or −0.23 V vs. SCE). 2) A more complex inner-sphere process initiated by the reaction given in Equation (4), followed by protonation of $[Pd_3(H)]^+$, subsequent reductive elimination of H_2 [Eq. (6)] and comproponation between $[Pd_3]^{2+}$ and $[Pd_3]^0$ [Eq. (7)], which is a familiar reaction in the redox chemistry of the Pd_3 cluster.[35] In agreement with the pathway given in Equation (6), we verified independently that addition of strong acids on $[Pd_3(H)]^+$ affords $[Pd_3]^{2+}$.

$$[Pd_3(H)]^+ + H^+ \rightarrow [Pd_3]^{2+} + H_2 \quad (6)$$

$$[Pd_3]^{2+} + [Pd_3]^0 \rightarrow 2[Pd_3] \quad (7)$$

Optimised geometry and MO analysis: The optimised geometries for the $[Pd_3(H)]^{n+}$ species ($n=+1$, 0, -1) were modeled by using $[Pd_3(H_2PCH_2PH_2)_3(\mu_3\text{-}CO)(\mu_3\text{-}H)]^{n+}$ with DFT methods (Table 2). For all three cases, the C_{3v} structure was obtained in agreement with the structures for the halogen adducts of $[Pd_3(dppm)_3(CO)]^{2+}$[27] and the corresponding Pt-analogue, $[Pt_3(dppm)_3(CO)(H)]^{+}$.[28] These data are interpreted using MO arguments.

Table 2. Selected bond lengths [Å] and angles [°] for the optimised geometries of the model $[Pd_3(H_2PCH_2PH_2)_3(\mu_3\text{-}CO)(\mu_3\text{-}H)]^{n+}$ compounds.

	$n=+1$	$n=0$	$n=-1$
d(Pd–Pd)	2.603	2.693	2.932
d(Pd–P)	2.385	2.404	2.410
d(Pd–C)	2.350	2.312	2.169
d(Pd–H)	2.027	2.027	1.975
d(C=O)	1.171	1.181	1.203
∢(Pd-H-Pd)	79.9	81.7	87.4

For $n=+1$, the computed Pd–Pd bond length (2.60 Å) is identical to that found for $[Pd_3(dppm)_3(CO)(X)]^{+}$ (X = Cl, Br, I).[27,36] Similarly, the Pd–H distance compares favourably to that experimentally determined for other bridged Pd–H species.[20] The representation of the HOMO and LUMO are provided in Figure 8 and a brief description of only relevant features are presented, as detailed descriptions of the frontier MO's for $[Pd_3]^{2+}$ and $[Pt_3]^{2+}$ species are reported elsewhere.[37–39]

The HOMO exhibits weak Pd–Pd bonding and antibonding Pd–H and Pd–CO interactions, which are also common for halide adducts of $[Pd_3]^{2+}$.[36] The LUMO is essentially M-based, and exhibits antibonding Pd–Pd interactions. The one-electron reduction of $[Pd_3(H)]^{+}$ leads to the $[Pd_3(H)]^{0}$ cluster placing this electron in an antibonding MO rendering the Pd–Pd bonding interactions weaker, as illustrated by the increase in d(Pd–Pd). The "unchanged" Pd–H bond length during this process is consistent with the absence of atomic contribution of the hydride. An additional one-electron reduction leads to a Pd–Pd bond order of 0 in $[Pd_3(H)]^{-}$, and the computed distance of 2.932 Å compares very favourably to that reported in the d^{10}–d^{10} $[Pd_2(dppm)_3]$ dimer (2.956(1) Å).[40] The presence of the dppm-bridging ligands prevents cluster dissociation, rendering the electrochemical processes chemically reversible. The fact that the Pd–H distance is still not very affected by this reduction process is again consistent with the nature of the LUMO. However, the large lability property of the hydride in this $[Pd_3(H)]^{-}$ adduct is solely responsible for explaining the dissociation.

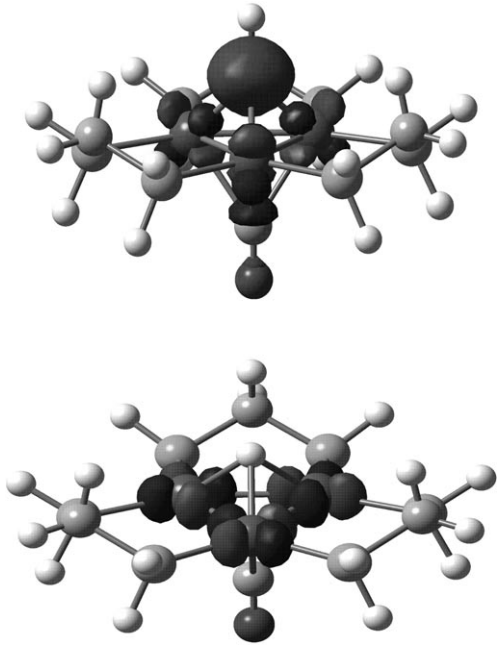

Figure 8. HOMO (top) and LUMO (bottom) drawings for $[Pd_3(H_2PCH_2PH_2)_3(CO)(H)]^{+}$.

Conclusion

This work focuses on the synthesis of a new trinuclear palladium–hydride cluster containing a $Pd_3(\mu_3\text{-}H)$ core. Three routes for its synthesis were investigated, but the most convenient and efficient one uses an organic formate. The electrochemical reduction of the hydride cluster $[Pd_3(H)]^{+}$ was also investigated and its reduction induces the loss of the hydride ion H^{-}.

Regarding the reactivity of the hydride cluster, preliminary results show that it is able to exchange its hydrogen atom with halogen X of organic RX compounds to afford $[Pd_3(\mu_3\text{-}X)]$ and R-H. Studies are in progress with the aim of development in hydrogen-transfer catalysis.

Experimental Section

Materials: $[Pd_3(dppm)_3(CO)][PF_6]_2$ was prepared according to a literature procedure.[41–43] Tetrahydrofuran (THF) was distilled over sodium/benzophenone under argon. The Bu_4NPF_6 salt was synthesised by mixing stoichiometric amounts of Bu_4NOH (40% in water) and HPF_6 (60% in water). After filtration, the salt was recrystallised twice in ethanol and dried at 80 °C during at least two days. The following materials were purchased from commercial suppliers without further purification: sodium borohydride (Avocado), tributylamine (Fluka) and formic acid (Carlo Erba).

Apparatus: NMR spectra were measured on a BRUKER 600 MHz Avance II and 500 MHz Avance DRX spectrometers (^{1}H and ^{2}H NMR: 300.15 MHz, ^{31}P NMR: 121.497 MHz) in Dijon. The reference was the residual non-deuterated solvent. The chemical shifts are reported with respect to TMS (^{1}H and ^{2}H NMR spectroscopy) and H_3PO_4 (^{31}P NMR spectroscopy). Mass spectra were obtained on a Bruker ProFLEX III spectrometer (MALDI-TOF) by using dithranol as matrix.

Stopped-flow experiments: The stopped-flow kinetic runs were carried out, at 15 °C, with a Hitech SF-61-DX2 apparatus coupled with a Hitech diode-array UV/Vis spectrophotometer. To minimise oxidation reactions in the stopped-flow apparatus, relatively concentrated cluster solutions ($2\times2.5.10^{-4}$ mol L^{-1}, ≈maximum solubility) were used. Under these conditions, the cell was kept at its smaller length (1.5 mm). The dead time was ≈1 ms. Kinetic runs were analysed with Specfit,[32] while the fitting

of the observed first-order rate and equilibrium constants was carried out with Excell Solver. The standard deviation on the determined parameters was obtained by using the Solver Aide macro. The cluster solution (5×10^{-4} mol L^{-1}) was mixed with formate-containing solution in a way that the concentration ratio, $R=[HCO_2^-]/[\text{cluster}]=10$, 20,…50. The data analysis was performed in a pseudo first-order ($R\geq10$) regime.

Electrochemical experiments: All manipulations were performed by using Schlenk techniques in an atmosphere of dry oxygen-free argon. The supporting electrolyte was degassed under vacuum before use and then dissolved to a concentration of 0.2 mol L^{-1}. For cyclic voltammetry experiments, the concentration of the analyte was almost 10^{-3} mol L^{-1}. Voltammetric analyses were carried out in a standard three-electrode cell EG&G Princeton Applied Research (PAR) Model 263 A potentiostat, connected to an interfaced computer that employed Electrochemistry Power Suite software. The reference electrode was a saturated calomel electrode (SCE) separated from the solution by a sintered glass disk. The auxiliary electrode was a platinum wire. For all voltammetric measurements, the working electrode was a vitreous carbon electrode ($\Phi=$ 3 mm). Under these conditions, when operating in THF, the formal potential for the ferrocene (+/0) couple was found to be +0.56 V versus the SCE. The controlled potential electrolysis was performed with an Amel 552 potentiostat coupled with an Amel 721 electronic integrator. High-scale electrolyses were performed in a cell with three compartments separated with fritted glasses of medium porosity. Carbon gauze was used as the working electrode, a platinum plate as the counter electrode and a saturated calomel electrode as the reference electrode.

Digital simulations of voltammograms within the framework of the reaction mechanisms specified in Scheme 2 were realised with commercial software DIGISIM 3.05 (Bioanalytical Systems). The potential step size was 5 mV. The value of the uncompensated resistance was taken as 2 kΩ. The double-layer capacitance value was estimated as $C_{dl}/A=1.7.10^{-4}$ F cm^{-2}. The standard potential (E_1^o and E_2^o), the heterogeneous rate constants (k_{h1} and k_{h2}) and the diffusion constant for $[Pd_3]^{2+}$ ($D=2.5.10^{-6}$ cm^2s^{-1}) were evaluated previously.[34] The charge transfer coefficients α_i was arbitrarily set at 0.5. The standard potential (E_3^o and E_4^o), the heterogeneous rate constants (k_{h3} and k_{h4}) and the diffusion constant for $[Pd_3(H)]^+$ ($D=3.5.10^{-6}$ cm^2s^{-1}) were then obtained by simulation of the RDE voltammogram (Figure 6a) and by comparison with that of $[Pd_3]^{2+}$.

$[Pd_3(dppm)_3(CO)(H)]PF_6$: $(Bu_3NH)(HCO_2)$ (solution prepared by mixing HCO_2H and NBu_3 in THF, 6.7 μmol) was added to a solution of $[Pd_3(dppm)_3(CO)][PF_6]_2$ (12 mg, 6.7 μmol) in THF (10 mL). The red reaction mixture immediately turned burgundy. Then, the solution was evaporated to dryness and the residue dissolved in deuterated acetone or THF, after concentration for the ^{2}H NMR analysis. ^{1}H NMR ([D$_6$]acetone): $\delta=$ 7.3–8 (m, 60H; Ph), 4.8, 4.9 ppm (br, 6H; P-CH_aH_b-P); ^{2}H NMR (THF): $\delta=3.1$ ppm (br s, hw = 19 Hz, μ_3-*H*); ^{31}P NMR ([D$_6$]acetone): $\delta=-12.7$ (d, ^2J(P,H) = 19–20 Hz; PH_2-*P*-CH_2), −144.2 ppm (hept, ^1J(P,F) = 712 Hz; *P*F_6^-); UV/Vis (THF): $\lambda_{max}=484$ nm; MS (MALDI-TOF): *m/z*: 1472 $[Pd_3(dppm)_3]$, 1088 $[Pd_3(dppm)_2]$, 982 $[Pd_2(dppm)_2]$.

Theoretical computations: Calculations with the density functional theory (DFT) approximation were performed by using the commercially available Gaussian 98 software.[44] The hybrid B3LYP exchange–correlation function was considered due to the high accuracy of the ensuing results,[45–47] with the 3–21G* as the basis set.[48–50] For the Pd atoms, the LANL2DZ effective core potential was used. Due to the great CPU time consuming of the dppm, it was replaced by the $PH_2CH_2PH_2$ bridging ligand. A symmetric C_{3v} structure was assigned as starting geometry and the computations were performed without symmetry constraint.

Acknowledgements

P.D.H. thanks the NSERC (Natural Sciences and Engineering Research Council) for funding. Y.M. is grateful to the CNRS (Centre National de la Recherche Scientifique) and the Conseil Régional de Bourgogne for funding.

[1] P. Tripodi, D. Di Gioacchino, R. Borelli, J. D. Vinko, *Phys. C* **2003**, *388–389*, 571–572.
[2] M. Perez Jigato, B. Coussens, D. A. King, *J. Chem. Phys.* **2003**, *118*, 5623–5634.
[3] N. K. Nag, *J. Phys. Chem. B* **2001**, *105*, 5945–5949.
[4] C. Gabrielli, P. P. Grand, A. Lasia, H. Perrot, *J. Electrochem. Soc.* **2004**, *151*, A1943 A1949.
[5] W.-S. Zhang, Z.-L. Zhang, X.-W. Zhang, *J. Electroanal. Chem.* **1999**, *474*, 130–137.
[6] W. S. Zhang, Z. L. Zhang, X. W. Zhang, *J. Electroanal. Chem.* **2000**, *481*, 13–23.
[7] T. Imokawa, G. Denuault, *Chem. Senses* **2004**, *20*, 106–108.
[8] L. Cser, G. Toeroek, G. P. Krexner, I. Sharkov, *Appl. Phys. Lett.* **2004**, *85*, 1149–1151.
[9] H. Araki, M. Nakamura, S. Harada, T. Obata, N. Mikhin, V. Syvokon, M. Kubota, *J. Low Temp. Phys.* **2004**, *134*, 1145–1151.
[10] K. Yamakawa, *J. Phys. Condens. Matter* **1999**, *11*, 8681–8688.
[11] W. Clegg, G. R. Eastham, M. R. J. Elsegood, B. T. Heaton, J. A. Iggo, R. P. Tooze, R. Whyman, S. Zacchini, *Organometallics* **2002**, *21*, 1832–1840.
[12] F. Ozawa, H. Okamoto, S. Kawagishi, S. Yamamoto, T. Minami, M. Yoshifuji, *J. Am. Chem. Soc.* **2002**, *124*, 10968–10969.
[13] W. Clegg, G. R. Eastham, M. R. J. Elsegood, B. T. Heaton, J. A. Iggo, R. P. Tooze, R. Whyman, S. Zacchini, *J. Chem. Soc. Dalton Trans.* **2002**, 3300–3308.
[14] M. S. Viciu, G. A. Grasa, S. P. Nolan, *Organometallics* **2001**, *20*, 3607–3612.
[15] M. A. Zuideveld, P. C. J. Kamer, P. W. N. M. Van Leeuwen, P. A. A. Klusener, H. A. Stil, C. F. Roobeek, *J. Am. Chem. Soc.* **1998**, *120*, 7977–7978.
[16] K. Tezuka, Y. Ishizaki, Y. Inoue, *J. Mol. Catal. A* **1998**, *129*, 199–206.
[17] G. Cavinato, M. Pasqualetto, L. Ronchin, L. Toniolo, *J. Mol. Catal. A* **1997**, *125*, 15–22.
[18] I. D. Hills, G. C. Fu, *J. Am. Chem. Soc.* **2004**, *126*, 13178–13179.
[19] I. del Rio, C. Claver, P. W. N. M. van Leeuwen, *Eur. J. Inorg. Chem.* **2001**, 2719–2738.
[20] V. V. Grushin, *Chem. Rev.* **1996**, *96*, 2011–2033.
[21] M. A. Gomez, B. Chen, D. L. Freeman, J. D. Doll, *Theory At. Mol. Clusters* **1999**, 309–325.
[22] I. Gauthron, J. Gagnon, T. Zhang, D. Rivard, D. Lucas, Y. Mugnier, P. D. Harvey, *Inorg. Chem.* **1998**, *37*, 1112–1115.
[23] D. Evrard, D. Meilleur, M. Drouin, Y. Mugnier, P. D. Harvey, *Z. Anorg. Allg. Chem.* **2002**, *628*, 2286–2292.
[24] D. Evrard, K. Groison, Y. Mugnier, P. D. Harvey, *Inorg. Chem.* **2004**, *43*, 790–796.
[25] D. Meilleur, D. Rivard, P. D. Harvey, I. Gauthron, D. Lucas, Y. Mugnier, *Inorg. Chem.* **2000**, *39*, 2909–2914.
[26] D. Meilleur, P. D. Harvey, *Can. J. Chem.* **2001**, *79*, 552–559.
[27] P. D. Harvey, Y. Mugnier, D. Lucas, D. Evrard, F. Lemaître, A. Vallat, *J. Cluster Sci.* **2004**, *15*, 63.
[28] B. R. Lloyd, R. J. Puddephatt, *J. Am. Chem. Soc.* **1985**, *107*, 7785–7786.
[29] B. R. Lloyd, L. Manojlovic-Muir, K. W. Muir, R. J. Puddephatt, *Organometallics* **1993**, *12*, 1231–1237.
[30] R. Provencher, K. T. Aye, M. Drouin, J. Gagnon, N. Boudreault, P. D. Harvey, *Inorg. Chem.* **1994**, *33*, 3689–3699.
[31] V. V. Grushin, C. Bensimon, H. Alper, *Organometallics* **1995**, *14*, 3259–3263.
[32] R. A. Binstead, B. Jung, A. D. Zuberbühler in Specfit/32, Vol. Spectrum Software Associates, Chapell Hill, NC, **2000**.
[33] I. Gauthron, Y. Mugnier, K. Hierso, P. D. Harvey, *Can. J. Chem.* **1997**, *75*, 1182.
[34] F. Lemaître, D. Lucas, D. Brevet, A. Vallat, P. D. Harvey, Y. Mugnier, *Inorg. Chem.* **2002**, *41*, 2368–2373.
[35] F. Lemaître, D. Lucas, K. Groison, P. Richard, Y. Mugnier, P. D. Harvey, *J. Am. Chem. Soc.* **2003**, *125*, 5511–5512.

[36] D. Lucas, F. Lemaître, B. Gallego-Gomez, C. Cugnet, P. Richard, Y. Mugnier, P. D. Harvey, *Eur. J. Inorg. Chem.* **2005**, 1011–1018.
[37] P. D. Harvey, R. Provencher, *Inorg. Chem.* **1993**, *32*, 61–65.
[38] R. Provencher, P. D. Harvey, *Inorg. Chem.* **1996**, *35*, 2113–2118.
[39] P. D. Harvey, S. M. Hubig, T. Ziegler, *Inorg. Chem.* **1994**, *33*, 3700–3710.
[40] R. U. Kirss, R. Eisenberg, *Inorg. Chem.* **1989**, *28*, 3372–3378.
[41] R. J. Puddephatt, L. Manojlovic-Muir, K. W. Muir, *Polyhedron* **1990**, *9*, 2767–2802.
[42] B. R. Lloyd, R. J. Puddephatt, *Inorg. Chim. Acta* **1984**, *90*, L77–L78.
[43] L. Manojlovic-Muir, K. W. Muir, B. R. Lloyd, R. J. Puddephatt, *J. Chem. Soc. Chem. Commun.* **1983**, 1336–1337.
[44] Gaussian 98 (Revision A.6), M. J. Frisch, G. W. Trucks, H. B. Schlegel, G. E. Scuseria, M. A. Robb, J. R. Cheeseman, V. G. Zakrzewski, J. A. Montgomery, R. E. Stratmann, J. C. Burant, S. Dapprich, J. M. Millam, A. D. Daniels, K. N. Kudin, M. C. Strain, O. Farkas, J. Tomasi, V. Barone, M. Cossi, R. Cammi, B. Mennucci, C. Pomelli, C. Adamo, S. Clifford, J. Ochterski, G. A. Petersson, P. Y. Ayala, Q. Cui, K. Morokuma, D. K. Malick, A. D. Rabuck, K. Raghavachari, J. B. Foresman, J. Cioslowski, J. V. Ortiz, B. B. Stefanov, G. Liu, A. Liashenko, P. Piskorz, I. Komaromi, R. Gomperts, R. L. Martin, D. J. Fox, T. Keith, M. A. Al-Laham, C. Y. Peng, A. Nanayakkara, C. Gonzalez, M. Challacombe, P. M. W. Gill, B. G. Johnson, W. Chen, M. W. Wong, J. L. Andres, M. Head-Gordon, E. S. Replogle, J. A. Pople, Gaussian, Inc., Pittsburgh, PA, **1998**..
[45] A. D. Becke, *J. Chem. Phys.* **1993**, *98*, 5648–5652.
[46] C. Lee, W. Yang, R. G. Parr, *Phys. Rev. B* **1988**, *37*, 785–789.
[47] B. Miehlich, A. Savin, H. Stoll, H. Preuss, *Chem. Phys. Lett.* **1989**, *157*, 200–206.
[48] K. D. Dobbs, W. J. Hehre, *J. Comput. Chem.* **1986**, *7*, 359–378.
[49] K. D. Dobbs, W. J. Hehre, *J. Comput. Chem.* **1987**, *8*, 861–879.
[50] K. D. Dobbs, W. J. Hehre, *J. Comput. Chem.* **1987**, *8*, 880–893.

Received: January 16, 2007
Published online: April 23, 2007

